Acoustic Emission for Characterization of Failure Mechanism in Textile Reinforced Mortar Laminates

Johan BLOM*, Michael EL KADI*, Jan WASTIELS*, Dimitrios G. AGGELIS*
*Department of Mechanics of Materials and Constructions, Vrije Universiteit Brussel, Pleinlaan 2, 1050 Brussels, Belgium

Abstract. This work presents the acoustic emission (AE) behaviour of textile reinforced cementitious composite laminates (TRC) under tensile and flexural loading. The aim is to connect specific AE parameters and indices to the different fracture mechanisms that are successively activated within the failure process of the complex composite material. These mechanisms include multiple matrix cracking at low load and fibre pull-out after the maximum load is reached. Interlaminar shear is also activated during bending depending on the thickness of the laminates. Preliminary analysis indicates that frequency and AE waveform shape parameters are shifting, following the shift of fracturing mechanisms. Since the heterogeneous fibrous nature and the plate specimen geometry are bound to result in wave dispersion, multiple sensors are used to investigate the effect of wave distortion due to propagation. It is concluded that while AE indices can adequately characterize the fracture process in real time, the sensor separation distance should be accounted for, in order to produce reliable characterization of the damage mechanism regardless of the sensors location.

1. Introduction

Acoustic emission is a technique used widely for health monitoring purposes of different structures and materials. Adequate sensors (usually piezoelectric) are attached on the surface of the material in order to record the response under the elastic excitation of the cracking sources [1]. The population and the parameters of the incoming signals are related to the ongoing processes and enable the monitoring of fracture from the onset until the final stages [2-5]. Fracture mechanisms like concrete matrix cracking and debonding of external patches, show different AE signatures enabling the evaluation of the fracture stage according to the load [6].

In this study textile reinforced cement (TRC) was the model material [7]. The specimens were made of inorganic phosphate cement (IPC) layers of glass fibers in random orientation [8]. This material is used as external reinforcement and repair of concrete structures and additionally it exhibits high resistance to fire. TRC members usually come in thin lightweight elements. This renders the prediction of its structural response not an easy task considering its laminated and fiber nature. Modeling of stress fields is complicated by

License: http://creativecommons.org/licenses/by/3.0/

interlaminar shear. In an effort to gain some understanding on the developed stress fields under different geometric conditions, thin beams of TRC were tested under three-point loading. The bottom span was variable; as the span decreases, the shear stresses are promoted relatively to the normal stresses, and damage to the laminar interphases becomes more likely. Fig. 1 shows schematically the dominant fracture mechanisms at low and high load due to bending. Initially, fracture is manifested by cracks of the matrix due to the tensile stresses. As load and deflection increase, the fibers bridging the cracks are being pulled out while at the points of discontinuity delaminations start to develop. Therefore, there is a shift between fracture mechanisms which is reasonable to trigger different AE signals. As has been shown, matrix cracks trigger mostly the first symmetric plate wave mode (S0) rather than the antisymmetric (A0) while delaminations increase the proportion of energy of A0 [9,10]. The relative change of the modes affects the shape of the received waveforms and the AE parameters, see Fig. 1. The most important waveform features are the amplitude, A, the rise time, RT, the RA-value which is RT over A. RT and RA have proven sensitive to the cracking mode, obtaining low values for tensile phenomena and higher for shear either in the form of delaminations or cracking due to shear stresses [3,5,6,11,12]. A usual frequency indicator is the average frequency, AF, which is the number of threshold crossings over the duration.

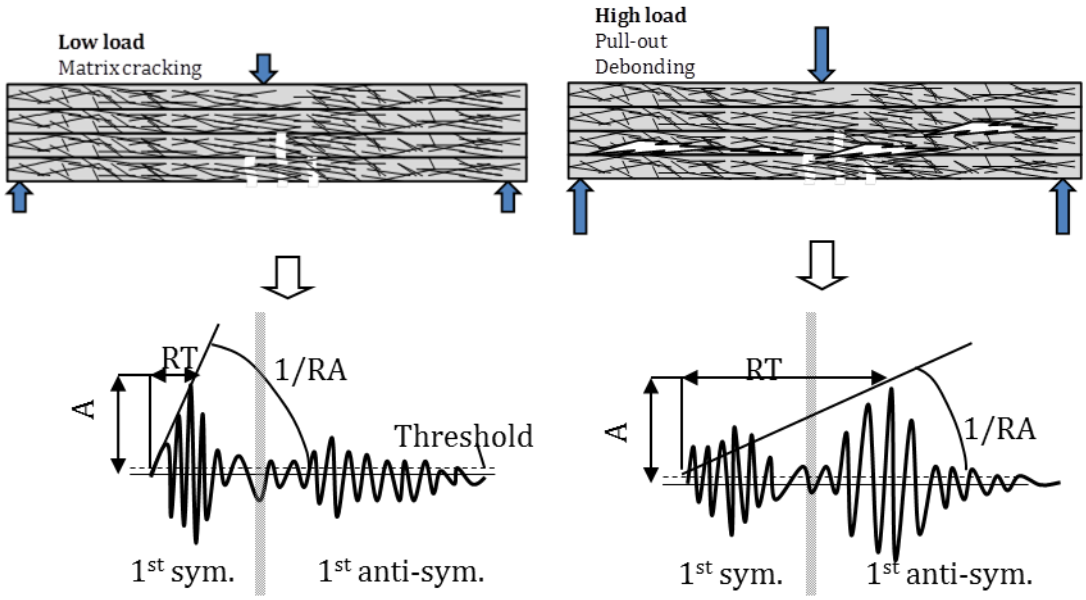

Fig. 1. Typical damage modes and their corresponding AE waveforms.

2. Experimental details

2.1 Materials and testing

The inorganic calcium phosphate (IPC) matrix is a mixture of a calcium silicate powder and a phosphoric acid based solution of metal oxides. The weight ratio of powder to liquid is 0.8. For the mixing a Heidolph RZR 2102 overhead mixer is used. E-glass chopped glass fibre mats with a surface density of 300 g/m² (Owens Corning M705-300) are used as reinforcement. All 8 layer IPC laminates are made by hand lay-up with an average matrix consumption of 800 g/m² for each layer, which results in an average fibre volume fraction (V_f) of 20%. Laminates are cured under ambient conditions for 24 hours. Post-curing is performed at 60°C for 24 hours while both sides are covered with plastic to prevent early

evaporation of water. The dimensions of the TRC specimens are: 350x50x4 mm. The laminates were loaded in a three-point bending test. In this case the span between the supports was set to: 330, 250, 150 and 60 mm leading to aspect ratios of 82.5, 62.5, 37.5 and 15. The test was performed using an Instron 5885H universal testing machine using a loading rate of 2 mm/min.

2.2 AE monitoring

The sensors (pico of Mistras Holdings) were broadband, with a central frequency of 450 kHz. In total five sensors were used, see Fig. 2. Two were placed 25 mm either way of the loading point. Multiple sensors were applied in order to monitor the same AE sources from different positions. In this paper the focus is given on the monitoring by the close-by sensors around the crack (e.g. 1 and 2) while the results of the others are also discussed. Vaseline grease was used for acoustic coupling and the sensors were secured by tape during the loading. The signals over the threshold of 35 dB were acquired in a micro-Samos board after pre-amplification of 40 dB with sampling rate of 10 MHz. Photographs of the setup can be seen in Fig. 3a and b for the longest span and the shortest span respectively.

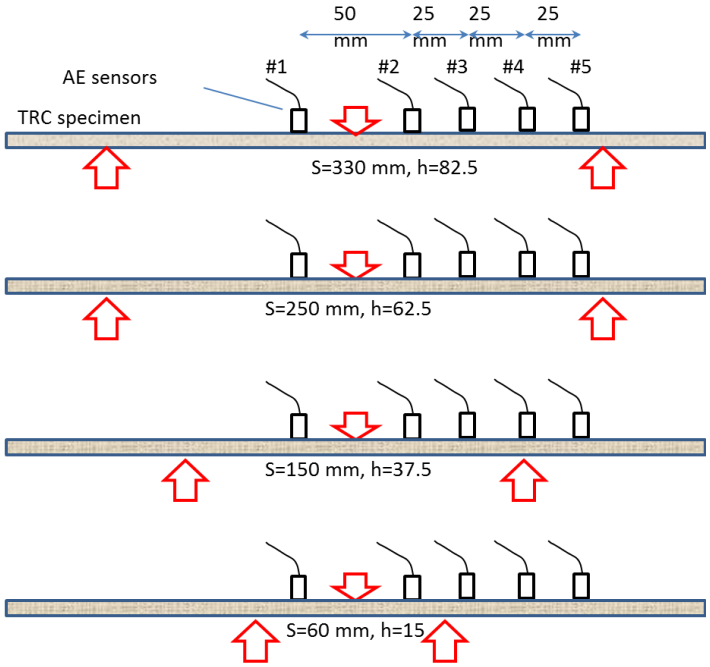

Fig. 2 Experimental setup and AE monitoring.

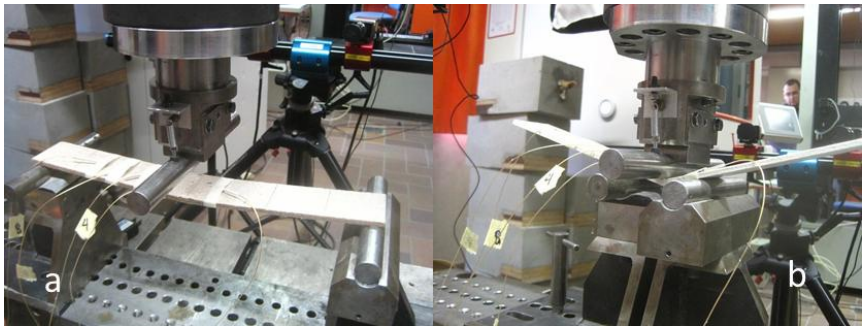

Fig. 3 Photographs of the test for beams with span (a) 330 mm and (b) 60 mm.

3. Mechanical results

The force vs. displacement curves from the three-point bending tests for the different beams are shown in figure 4. As the span is shortened the maximum load increases which is normal due to the lower bending moment and consequently the lower stresses developed. On the other hand, the test of the long spans lasted more since they could undertake high ultimate deflection compared to the span of 60 mm.

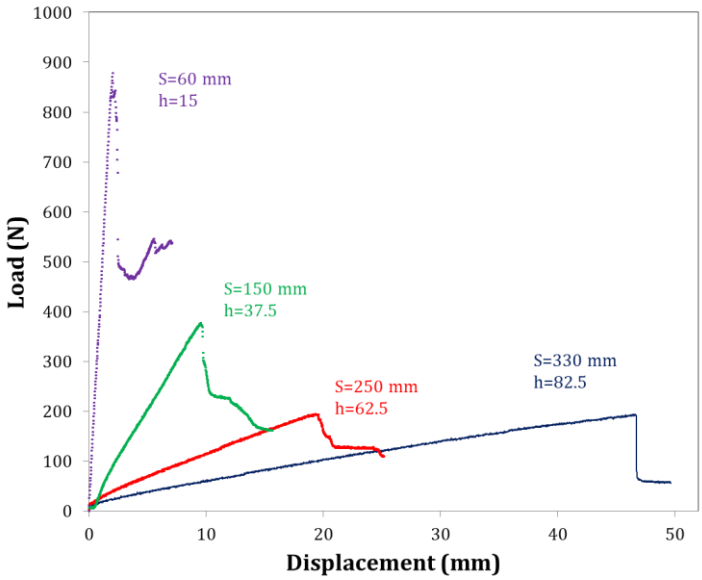

Fig. 4. Force vs. time curves for 8 layer TRC laminates with different span in three-point bending.

4. AE results

The comparison of the total activity of the four beams showed that the short span exhibited far more AE during testing, while it quickly reached a constant rate. On the other hand the longest span showed a continuously increasing rate up to a point of burst when macroscopic fracture created a large part of the activity within a few seconds [13]. In this paper the focus is given on the qualitative waveform parameters of AE. Important information is included in the characteristics of the waveforms. Since the specimen geometry is dispersive and the material is heterogeneous, the results below are from a single sensor and specifically #2 (Fig. 2), which is closer to the middle. This way the propagation effect is the minimum possible and similar for all geometries. Therefore, any different trends can be safely attributed to the different loading conditions, i.e. different span. Later results from other distances are discussed to show the effect of additional propagation.

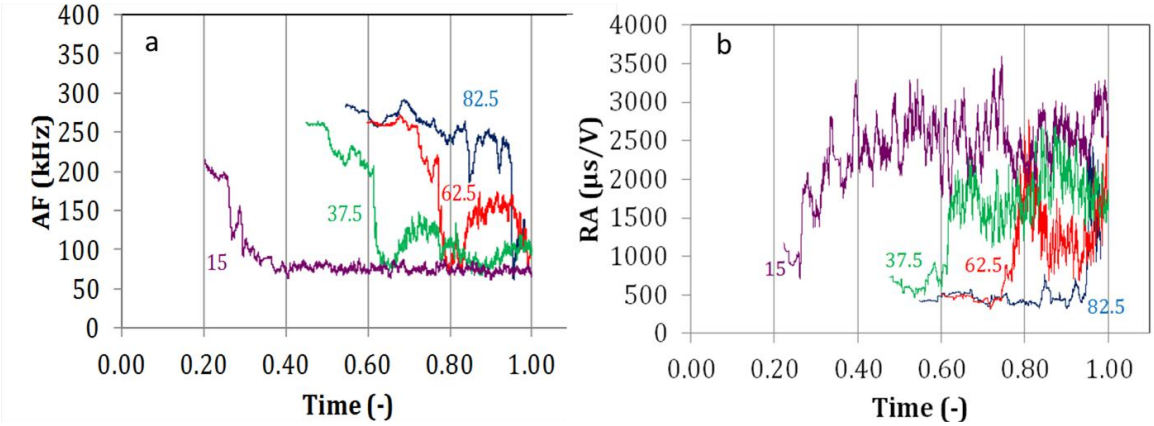

Fig. 5 AF moving average during bending of TRC beams of different aspect ratios (span over thickness) as received by sensor #2 at 25 mm from the center.

Fig. 5a shows the AF as a moving average of 300 hits received by sensor #2 in all beams. Since the duration of the experiments was different, the time scale is normalized to maximum. As mentioned earlier the fracture sequence consists of initial matrix cracking, followed by pull-out and delamination. Therefore, a transition from high to low values of frequency would be expected in all beams. This is indeed shown in Fig. 5a. However, it is interesting to note that the shift occurs at different relative times. Starting from the long span (h=82.5) the AF line stays at approximately 250 kHz until just before the catastrophic failure that eventually occurred. This signifies that the main active mechanism was constant for most of the duration of the experiment and finally after the load drop, the next mechanism (debonding) was activated producing frequencies of 100 kHz in average. As we move to shorter spans, this transition occurs much earlier, indicating that this transition between matrix cracking and shearing occurred earlier in the loading. For the shortest span of aspect ratio 15 the initial value is at approximately 200 kHz, much lower than the long span, and the downshift comes quite early (in fact less than a minute into the loading). It implies that the matrix cracking is saturated very early giving its place to fiber pull-out and debonding which were active throughout the rest of the experiment. Fig. 5b shows the corresponding curves for RA value. The long span remained at low levels for almost the whole duration of the experiment (approx. 500 μs/V) confirming that matrix cracking was the dominant mechanism for most of the loading. At the end and the point of macroscopic failure the RA exhibited an explosive increase to 2000 μs/V. As the span is shortened, this transition occurs again much earlier, while the initial RA value is around 1000 μs/V approximately double than the initial RA from the long span. Both AF and RA behaviors show that passive monitoring by AE has the potential to characterize the condition of the material in terms of its fracturing stage, giving valuable insight to the designers on how the material responds to the stress field. It is mentioned here that FEM analysis was also conducted to check the stress field in all four geometries. In the short span, due to lower bending moments the ratio of maximum normal stress to maximum shear is much lower than the long span. This difference in the applied stress field is reasonable to promote different fracture mechanisms (debonding for short spans and cracking for long ones) as seen by the different behavior of the AE descriptors.

In a preliminary effort to check the differences between AE from cracking and debonding in TRC two specific parts of the populations were isolated. One was the initial 300 hits when the load is still quite low and in all cases the basic mechanism behind AE is matrix cracking. The other group was the last 300 hits when the beam has failed macroscopically and the major mechanism is fiber pull-out and layer debonding. The populations were isolated for all the different sensors in order to obtain also the influence of the propagation distance on the characteristics of AE.

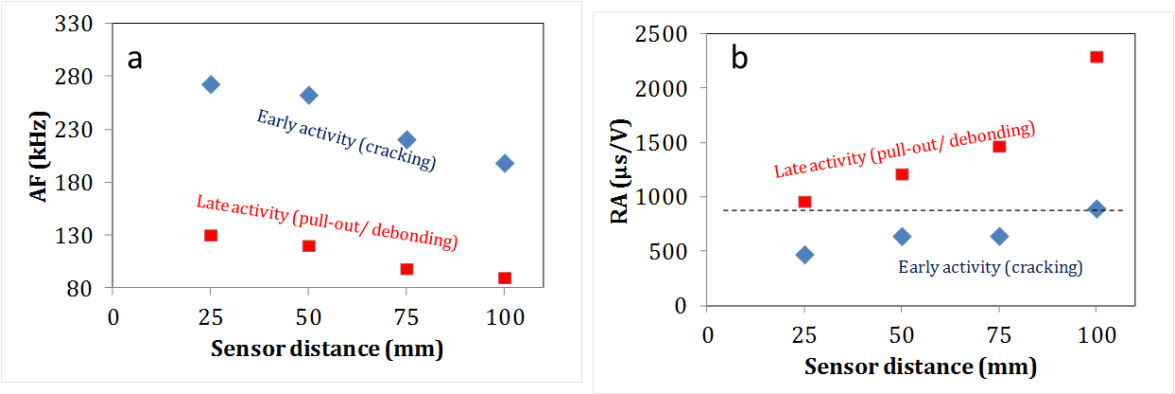

Fig. 6. (a) AF and (b) RA value vs. sensor distance for the span of 330 mm (aspect ratio of 82.5).

Fig. 6a shows the average value of AF for both the early and late activities. For sensor #2 (distance of 25 mm) there is a considerable difference since cracking averages around 270 kHz and debonding around 130 kHz in AF. These values do not remain constant for the next sensors though. For the signals received by further transducers the AF strongly decreases reaching values around 200 kHz for cracking and 85 kHz for shearing.

Concerning RA, the corresponding values are seen in Fig. 6b. For the closest sensor the average RA values for cracking and debonding are 500 and 1000 μs/V respectively, these values change strongly for further sensors. Indicatively the RA values move to 900 and 2300 μs/V for cracking and debonding respectively. This shows the tremendous effect of plate wave dispersion, damping and scattering on the waveforms. Since these shifts are registered for additional propagation distances of less 75 mm, the effect is expected huge in larger size structures.

The above mentioned trends show that as the propagation distance increases a cracking event starts to resemble a shear that propagated less. As an example a typical cracking waveform received by a sensor 100 mm away, exhibits the same RA with a shear 25 mm from the sensor (indicated by the dashed line in Fig. 6b). This would certainly hinder successful classification if the propagation distance is not taken into account. It would introduce a certain level of error due to the differential effect of distortion (some signals would suffer strong distortion and some others weak). However, if the AE signals are treated separately for each sensor, this would possibly decrease this error as in a recent case in mortar [14].

5. Conclusions

In this study the bending behavior of TRC laminates was monitored by AE. Results showed that by changing the loading conditions, as defined by different spans in the three point bending test, the AE parameters exhibit considerable differences. For short spans that promote shear stresses, the AE frequency content decreases and the duration and rise time of the emissions increase. This is very encouraging for further study concerning the evaluation of the dominant stress field in thin laminated composite structures from TRC, the mechanical modeling of which under complex loading is difficult. Furthermore since the differences in AE behavior are evident from the early activity of the first few hundreds of hits, this implies that a proof loading at low levels would actually give reliable predictions on the way the laminate will fracture. One important limiting issue is the waveform distortion due to wave propagation in a thin heterogeneous plate geometries. As a result, cracking signals lose frequency and become elongated in time resembling shear ones, something that would decrease the characterization success if the sensor distance is not accounted for.

References

[1] Grosse CU, Ohtsu M. "Acoustic emission testing". Heidelberg: Springer; (2008).

[2] Carpinteri A, Corrado M, Lacidogna G. "Heterogeneous materials in compression: Correlations between absorbed, released and acoustic emission energies," Engineering Failure Analysis 33, 236–250 (2013).

[3] T. Shiotani, Y. Oshima, M. Goto, S. Momoki. (2013) Temporal and spatial evaluation of grout failure process with PC cable breakage by means of acoustic emission, Construction and Building Materials 48, 1286-1292

[4] Muralidhara S, Prasad BKR, Eskandari H, Karihaloo BL. Fracture process zone size and true fracture energy of concrete using acoustic emission. Constr Build Mater 2010;24(4):479–86.

[5] Kawasaki, Y., Wakuda, T., Kobarai, T., Ohtsu, M., "Corrosion mechanisms in reinforced concrete by acoustic emission," Construction and Building Materials 48, 1240–1247 (2013).

[6] Aggelis, D.G., Verbruggen, S., Tsangouri, E., Tysmans, T., Van Hemelrijck, D.,"Characterization of mechanical performance of concrete beams with external reinforcement by acoustic emission and digital image correlation," Construction and Building Materials 47, 1037–1045 (2013).

[7] Brameshuber W, editor. Textile reinforced concrete. State-of-the-art report of RILEM Technical Committee 201-TRC; 2006.

[8] Blom J., Van Ackeren J., Wastiels J., Forming thermoplastic prepregs in a textile reinforced inorganic phosphate cement composite mould, Edition:SAMPE EUROPE SEICO 13 Conference Paris, pp: 467 - 473, eds: Mark A. Erath, published by: Mark A. Erath, published at: CH 4125 Riehen / Basel, ISBN-ISSN: 978-3-9523565-8-6, 2013.

[9] M. Eaton, M. May, C. Featherston, K Holford, S Hallet and R Pullin. Characterisation of Damage in Composite Structures using Acoustic Emission, Journal of Physics: Conference Series Volume 305 Number 1, 012086 doi:10.1088/1742-6596/305/1/012086.

[10] J.J. Scholey, P.D. Wilcox, M.R. Wisnom, M.I. Friswell, Quantitative experimental measurements of matrix cracking and delamination using acoustic emission, Composites Part A: 41 (2010) 612–623.

[11] Farhidzadeh, A., Salamone, S., Singla, P., "A probabilistic approach for damage identification and crack mode classification in reinforced concrete structures," Journal of Intelligent Material Systems and Structures 24(14), 1722-1735 (2013).

[12] Shahidan, S., Pulin, R., Muhamad Bunnori, N., Holford, K.M., "Damage classification in reinforced concrete beam by acoustic emission signal analysis," Construction and Building Materials 45, 78–86 (2013).

[13] D. G. Aggelis, J. Blom, M. El Kadi, J. Wastiels, Influence of geometry on the fracturing behavior of textile reinforced cement monitored by acoustic emission Proc. SPIE 9063, Nondestructive Characterization for Composite Materials, Aerospace Engineering, Civil Infrastructure, and Homeland Security 2014, 90630E (25 April 2014); doi: 10.1117/12.2044671, ISBN 9780819499899, 25/4/2014.

[14] A. Farhidzadeh, A. C. Mpalaskas, T.E. Matikas, H. Farhidzadeh, D. G. Aggelis, Fracture Mode Identification in Cementitious Materials using Supervised Pattern Recognition of Acoustic Emission Features, Construction and Building Materials, 10.1016/j.conbuildmat.2014.05.015.